1448 *KSME International Journal, Vol. 16 No. 11, pp. 1448~1456, 2002*

The Self-Induced Oscillations of the Under Expanded Jets Impinging Upon a Cylindrical Body

Heuy-Dong Kim*
School of Mechanical Engineering, Andong National University,
388 Songchun-dong, Andong, Kyungbuk 760-749, Korea
Hideo Kashimura
Department of Control and Information Systems Engineering, Kitakyushu College of Technology, Japan
Toshiaki Setoguchi
Department of Mechanical Engineering, Saga University, 1 Honjo-machi, Saga 840-8502, Japan

The present study addresses the flow characteristics involved in the self-induced oscillations of the underexpanded jet impinging upon a cylindrical body. Both experiment and computational analysis are carried out to elucidate the shock motions of the self-induced oscillations and to find the associated major flow factors. The underexpanded sonic jet is made from a nozzle and a cylindrical body is placed downstream to simulate the impinging jet upon an obstacle. The computational analysis using TVD scheme is applied to solve the axisymmetric, unsteady, inviscid governing equations. A Schlieren system is employed to visualize the self-induced oscillations generated in flow field. The data of the shock motions are obtained from a high-speed video system. The detailed characteristics of the Mach disk oscillations and the resulting pressure variations are expatiated using the time dependent data of the Mach disk positions. The mechanisms of the self-induced oscillations are discussed in details based upon the experimental and computational results.

Key Words : Underexpanded Jet, Jet Impingement, Supersonic Flow, Mach Disk, Compressible Flow, Unsteady Flow, Self-Induced Oscillation

1. Introduction

The underexpanded sonic or supersonic jet which impinges upon an obstacle has been applied to a variety field of aerospace technologies and industrial manufacturing processes and has often produced the self-induced oscillations in a flow field. This kind of flow oscillation is usually associated with unsteady motion of the shock wave in front of the obstacle, turbulence, and shear layer instability, causing a strong noise and vibration problem. The shock motions consist of low frequency-large amplitude components, compared with the oscillation components with regard to the turbulence and shear layer instability.

The flow field which supersonic jet impinges on an obstacle is highly complicated and fully three dimensional, almost always accompanying a considerable scale of unsteadiness. Many works have been carried out to understand the interaction physics between a supersonic jet and an obstacle (Lamont and Hunt, 1980; Jennions and Hunt, 1980; Gummer and Hunt, 1974; Iwamoto, 1990; Nishida and Matsumura, 1994). A time-mean behavior of the impinging jet is well known. For instance, the plate shock upstream of the obstacle, Mach disk and barrel shock are known well (Lamont and Hunt, 1980; Jennions and Hunt, 1980; Gummer and Hunt, 1974). Moreover

* Corresponding Author,
E-mail : kimhd@andong.ac.kr
TEL : +82-54-820-5622; **FAX** : +82-54-841-1630
School of Mechanical Engineering, Andong National University 388 Songchun-dong, Andong, Kyungbuk 760-749, Korea. (Manuscript **Received** April 16, 2001; **Revised** August 16, 2002)

the separation bubble and reattachment formed on the impinging area of the obstacle are clarified by flow visualization (Lamont and Hunt, 1980; Jennions and Hunt, 1980; Gummer and Hunt, 1974; Iwamoto, 1990; Nishida and Matsumura, 1994). With these time-mean data alone, no information can be deduced about the oscillation data, and understanding of how the time-mean data are generated is of practical importance in estimating wall loads and thereby in design of flow devices, since generally the underexpanded impinging jets are interpreted through them.

Unfortunately the time-dependent flow behavior of the underexpanded impinging jet is not well understood to date. Only a few work has been done to elucidate the self-induced oscillations of the underexpanded impinging jet (Powell, 1988; Jungowski, 1978; Kim et al., 2001a). Recently some work has been carried out to investigate the flow mechanisms involved in self-induced oscillations in the underexpanded impinging sonic jets and has revealed that the self-induced oscillations were mainly due to unsteady shock motions in front of the obstacle (Kim et al., 2001b).

However there are still many unsolved problems; what parameters drive the shock to oscillate in front of the obstacle? At what conditions do the self-induced oscillations occur? How are the position and size of the obstacle linked with the self-induced oscillations? What kind of strategy should be applied to suppress such undesirable oscillations, etc. There are countless other questions about the self-induced oscillations. The above list, though it is little more than the tip of an iceberg, can give some indication of the opportunities, which exist for future investigations.

The objective of the present study is to characterize the self-induced oscillations of the under expanded jet impinging upon a cylindrical body, to find major factors influencing the self-induced oscillations, and thus to give an insight into a proper means to suppress the self-induced oscillations. The underexpanded sonic jet is made from a nozzle and a cylindrical body is placed downstream to simulate the impinging jet upon an obstacle. The computational analysis using TVD scheme is applied to solve the axisymmetric, unsteady, inviscid governing equations. An experimental work is also made to validate the computational results. A Schlieren system is employed to visualize the self-induced oscillations generated in flow field.

2. Compuational Analysis

The flow field of a typical sonic jet impinging upon a cylindrical body is schematically shown in Fig. 1. The sonic jet exhausting from the nozzle having a diameter of D_e accelerates to a supersonic speed downstream of the exit of nozzle and decelerates to a subsonic speed by the shock wave having the Mach disk of a diameter of d_m which locates at the distance x_m from a nozzle exit. The resulting subsonic flow impinges on the cylindrical body of a diameter d_c, locating at the distance x_c from the nozzle exit.

Along the axis of the nozzle the pressure steeply rises due to the Mach disk, as is also schematically shown in Fig. 1. It is assumed that the pressures just upstream and downstream of the Mach disk are p_i and p_m, respectively. The flow behind the Mack disk is compressed, and the pressure steeply rises again up to p_d as the flow

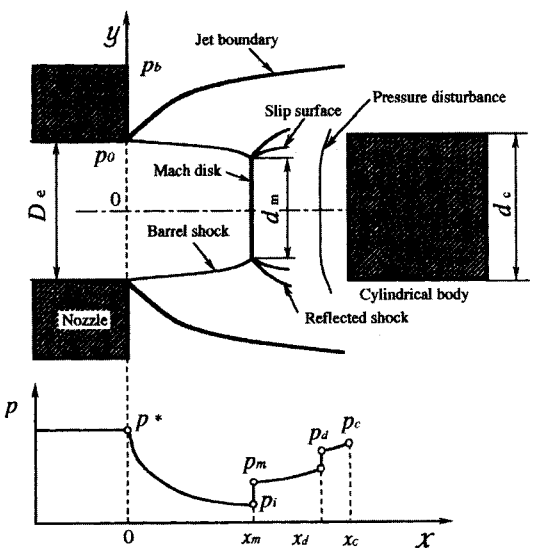

Fig. 1 Flow field of the underexpanded impinging jet

meets a pressure disturbance or a plate shock in front of the cylindrical body. Finally pressure p_c will be formed at the stagnation point of the cylindrical body.

Considering the x-y cylindrical coordinate system originated at the center of the nozzle exit, the governing equation systems are the compressible, unsteady, axisymmetric, Euler's equation, given by the conservation forms next.

$$\frac{\partial U}{\partial t}+\frac{\partial F}{\partial x}+\frac{\partial G}{\partial y}+W=0 \tag{1}$$

where

$$U=\begin{bmatrix}\rho'\\ \rho'u'\\ \rho'v\\ e'\end{bmatrix},\ F=\begin{bmatrix}\rho'u'\\ \rho'u'^2+p'\\ \rho'u'v'\\ (e'+p')u'\end{bmatrix},$$
$$G=\begin{bmatrix}\rho'v'\\ \rho'u'v'\\ \rho'v'^2+p'\\ (e'+p')v'\end{bmatrix},\ W=\frac{1}{y'}\begin{bmatrix}\rho'v'\\ \rho'u'v'\\ \rho'v'^2\\ (e'+p')v'\end{bmatrix} \tag{2}$$

The properties with symbol $'$ denote the non-dimensional quantities which are normalized by the nozzle exit diameter D_e and the supply conditions of pressure p_o, density ρ_o, and speed of sound a_o at the nozzle inlet. Equation (1) is solved using the second-order symmetric Total Variation Diminishing(TVD) method (Yee, 1987) with the operator splitting technique (Sod, 1977). The square grid system is used and the time step Δt is decided by the CFL condition. For simplicity of the present computations, the sonic jet conditions are assumed at the nozzle exit, M_e= 1.0. Further assumptions are made; the ratio of specific heats κ=1.4, the diameter of a cylindrical body $d_c=D_e$ and the position $x_c=2D_e$. The detailed boundary conditions (Kim et al., 2001b) used in the present computations are described in Fig. 2. The pressure ratio of the reservoir pressure p_o and back pressure p_b is varied in the range of $2\leq\phi(=p_o/p_b)\leq 20$.

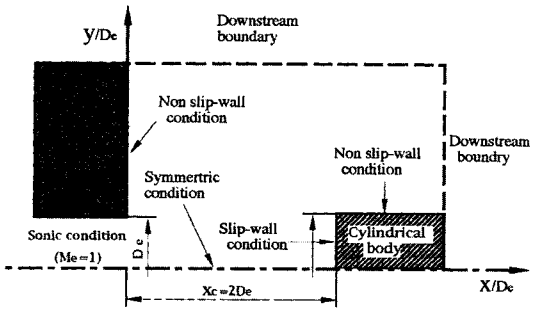

Fig. 2 Flow Field for computation

3. Experimental Work

The schematic layout of the present experimental facility and measurement systems is illustrated in Fig. 3. The nozzle and cylindrical body are placed inside the test chamber, which has an optical window for flow visualization. The test chamber is so large that it does not interference with the impinging jet. A convergent nozzle with the exit diameter of D_e=4 mm is to obtain the underexpanded sonic jets in the test chamber. A cylindrical body of a diameter of $d_c=D_e$ is placed downstream of the nozzle. The location x_c of the cylindrical body is varied between $1D_e$ and $4D_e$.

The compressed, dry air is employed as a test gas and the pressure ratio ϕ is varied in the range of $3\leq\phi(=p_o/p_b)\leq 20$. A pressure control valve is installed upstream of the plenum chamber to get a nozzle supply pressure needed. The plenum supply pressure upstream of the nozzle is monitored to ensure that it is kept constant during the test.

The impinging jet flow is visualized by a Schlieren system, which is equipped with a high-

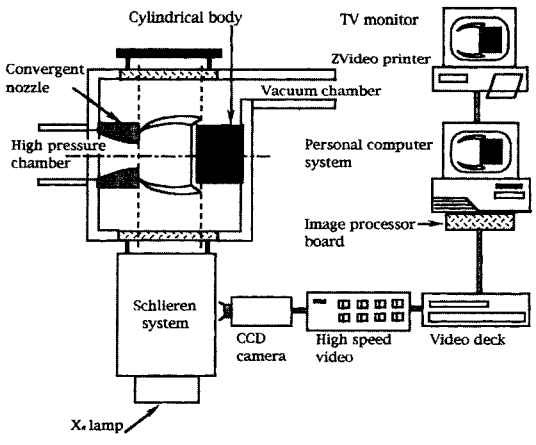

Fig. 3 Experimental facility and flow visualization system

speed video camera (Photoron Inc., HVC-11B). The system is capable of scanning the instantaneous images at the rate up to 2066 frames/s. Digitized data of the brightness of the Schlieren image is transmitted to PC via an image processing board (Photoron Inc., FDM98-4). The data of flow visualizations give the instantaneous displacement of Mach disk which is generated inside the underexpanded jet. Detailed measurement technique is referred to the previous work (Kim et al., 1992).

4. Results and Discussions

For the pressure ratios of ϕ=5.5 and 9.0 the typical Schlieren pictures are shown in Fig. 4. The flow is from left to right. The underexpanded jet from the nozzle impinges on a cylindrical body. Some turbulence structures are found around the cylindrical body. The Mach disk upstream of the cylindrical body, barrel shocks and reflected shocks are observed in these pictures.

It is found from the optical observation that the flow is highly unstable at a certain pressure ratio and location of the cylindrical body. Figure 5 presents the regime of the self-induced oscillations of the impinging jet flows. Figure 5(a) shows the ranges of ϕ and x_c/D_e where the Mach disk oscillates in front of the cylindrical body. The experimental data show both the upper ϕ_{up} and lower limits ϕ_{low} of the pressure ratio where the self-induced oscillations are observed for each location of the cylindrical body. The hatched region indicates the regime of the self-induced oscillations.

For a given location of the cylindrical body

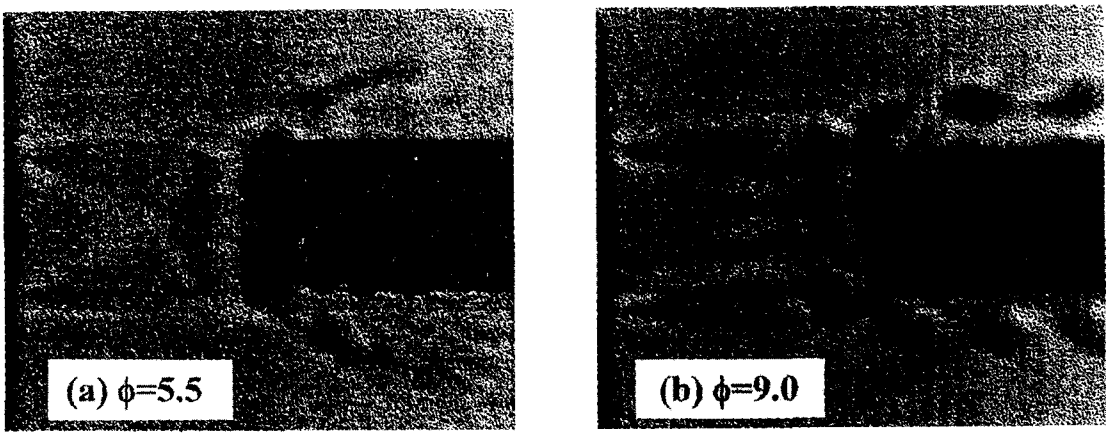

Fig. 4 Schlieren pictures showing the underexpanded impinging jets

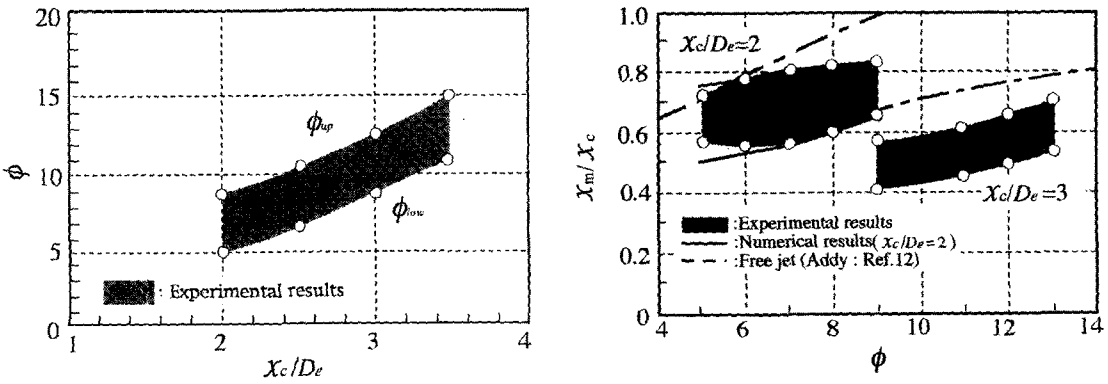

(a) x_c/D_e vs ϕ for Mach disk oscillations (b) x_m/x_c vs ϕ for Mach disk oscillations

Fig. 5 Regime of Mach disk oscillations

there is a certain range of the pressure ratio for self-induced oscillations. For instance, the self-induced oscillations are generated in the range of $2 \leq x_c/D_e \leq 3.5$. It seems that the pressure ratio for the self-induced oscillations is $5 \leq \phi \leq 9$ at $x_c/D_e=2.0$, and $9 \leq \phi \leq 13$ at $x_c/D_e=3.0$, respectively. Thus it is evident that the pressure ratio in which the self-induced flow oscillations occur increases with x_c/D_e.

Figure 5(b) shows the locations of Mach disk x_m/x_c during the self-induced oscillations. The ratio x_m/x_c means the upper and lower limits of the Mach disk positions in the region between the nozzle exit and cylindrical body. The lower limit means that the Mach disk locates nearly at the cylindrical body, the upper limit is when it locates nearly at the nozzle exit. Therefore, the hatched region indicates the possible regimes of the Mach disk oscillations observed during the test.

The solid line represents the present computational predictions and the dashed line shows the relation of the free jet obtained by Addy (1981). It seems that the present computations predict the experimented data with fairly good accuracy. The positions of Mach disk for the self-induced oscillations are in the range of $0.5 \leq x_m/x_c \leq 0.8$ at $x_c/D_e=2.0$ and $0.4 \leq x_m/x_c \leq 0.7$ at $x_c/D_e=3.0$, respectively. It seems that the Mach disk moves upstream from the cylindrical body toward the nozzle exit as x_c/D_e increases. From the comparison with the results of free jet, it is found that the Mach disk for the impinging jets locates more upstream, compared with the corresponding free jet.

For $x_c/D_e=2.0$ and $\phi=5.5$ the predicted density contours at several instants during a cycle of the self-induced oscillations are shown in Fig. 6. Since the density contours are presented by the black-white instead of colors, the light and black areas of the density contours may not be directly proportional to the real value of density, but just show density variation during a cycle of self-induced oscillations. Here, t' denotes a normalized time defined by $t'=t/(\sqrt{k}D_e/a_o)$ and T is a period of the self-induced oscillation.

It seems that the density contours considerably vary with time t'. At $t'=1/8$T, the Mach disk occurs near the cylindrical body. For time to increase, the Mach disk seems to move upstream toward the exit of the nozzle. At $t'=5/8$T, it

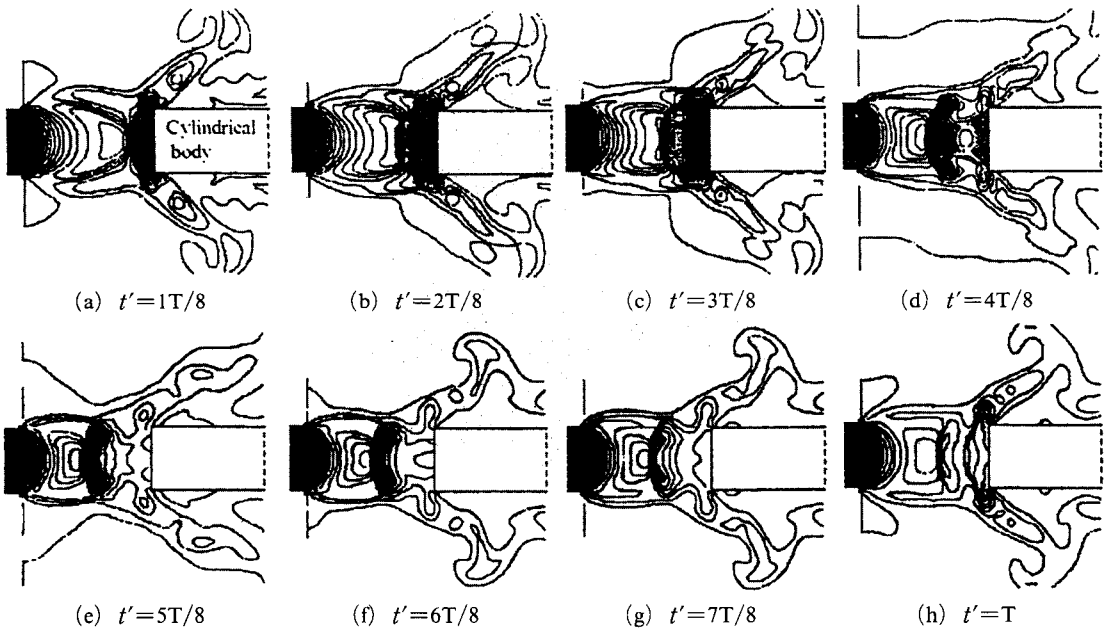

Fig. 6 Computed density contours at several instants during a cycle of the self-induced oscillations ($x_c/D_e=2.0$ and $\phi=5.5$)

seems to locates most upstream. Then the Mach disk moves downstream toward the cylindrical body with time.

It is interesting to note that the diameter of the Mach disk varies as it moves upstream or downstream. For instance, at $t'=6/8T$ and $t'=7/8T$, the diameter of the Mach disk seems to reduce as it moves toward the cylindrical body. At $t'=T$, a compression region is formed in front of a cylindrical body, leading to a plate shock there. This is resulted from coalescence of the compression region with the Mach disk. However it is observed at $t'=2/8T$ that the compression region and Mach disk are separated again from the plate shock.

The resulting new pressure waves are formed outside the jet boundary, propagating back ward the nozzle exit. From (c) to (g), the pressure waves are reflected from the nozzle exit, propagating downstream toward the cylindrical body with a decrease in the strength. In (h), the other new pressure waves occur at the nozzle exit. It is found from (c) to (e) that the density of the compression region decreases with an increase in time t' and the Mach disk moves toward the nozzle exit with a decrease in its diameter.

Figure 7 shows the change of the Mach disk diameter d_m/D_e during a cycle of oscillation. The points of (a) to (h) correspond to the flow states shown in Fig. 6. The data are obtained by the present computations for $x_c/D_e=2.0$ and $\phi=5.5$. It is known that d_m/D_e varies between 0.2 to 0.75 times the diameter of the nozzle exit, and its value strongly depends on the movement direction of the Mach disk at a fixed x_c/D_e. This results from the fact that the shock movement is associated with the pressure waves propagating outside of the jet boundaries.

Figure 8 shows the predicted pressure distributions along the nozzle axis during a cycle of oscillation for the same conditions as in Fig. 7. Here p_c' is the normalized pressure at the stagnation point of the cylindrical body. The plate shock is formed by coalescence the compression region with Mach disk. At $t'=3/8T$, p_i' and p_m' indicate the pressures just before and behind the Mach disk, respectively. Thus the sudden rise in

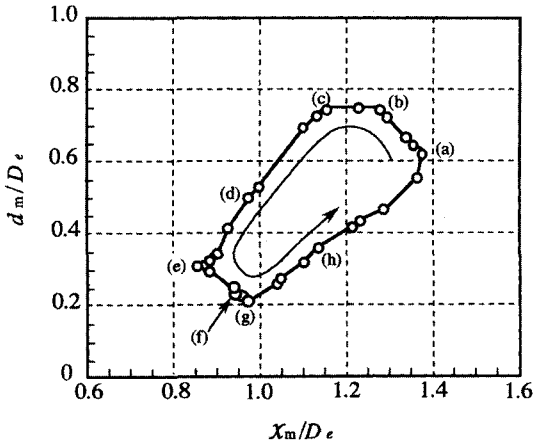

Fig. 7 Variation of Mach disk diameter during a cycle of the self-induced oscillations ($x_c/D_e=2.0$ and $\phi=5.5$)

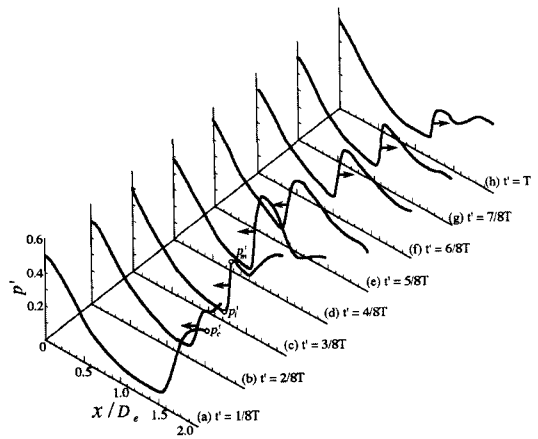

Fig. 8 Computed pressure distributions along the nozzle axis at several instants during a cycle of the self-induced oscillations ($x_c/D_e=2.0$ and $\phi=5.5$)

pressure from p_i' to p_m' is due to the Mach disk. It is very likely that at $t'=2/8T$, the compression region and Mach disk start to be separated from the plate shock. It seems that p_m' increases with time, but it decreases again at $t'=5/8T$, consequently leading to the decrease in p_c'.

At $t'=6/8T$, the Mach disk moves downstream toward the cylindrical body and the pressure in the region between the Mach disk and cylindrical body decreases from p_m' to p_c' continuously. p_m' decreases with time and p_c' increases again due to the reoccurrence of the compression region.

Figure 9 shows the relationship among p_m', x_m/D_e, and p_c'. It is found from Fig. 9(a) that p_m' strongly depends not only on the position of the Mach disk, but also on the direction of its movement. p_m' is increased as the Mach disk moves upstream, and decreased as the Mach disk moves downstream. For a given value of x_m/D_e, there are two different values of p_m'. In Fig. 9(b), the Mach disk movement also affects p_c'. This p_c' is increased as p_m' decreases and decreased as the p_m' increases. From the Mach disk locations, it is found that $p_c'>p_m'$ as the Mach disk locates near the cylindrical body and $p_c'<p_m'$ as the Mach disk locates near the nozzle exit. There is always an unbalance in the pressure during the self-induced oscillations. It is, therefore, reasonable to conclude that the self-induced oscillations are produced by unbalance of the pressure.

The predicted density contours for $\phi=3$ and $\phi=9$ are shown in Fig. 10. For $\phi=3$, the cell-structures of the jet are due to the compression and expansion waves impinging upon the jet boundaries. The Mach disk and barrel shock are clearly observed for $\phi=9$. Compared with the previous case of $\phi=5.5$, the diameter of the Mach disk seems to be much larger, but for $\phi=9$ the compression region just behind the Mach disk does not seem to occur in front of the cylindrical body.

Figure 11 shows the time histories of the pressure on the axis for the conditions of $\phi=3$ and 9. This plot gives the instantaneous locations of the Mach disk and the pressure waves as well, just like a conventional streak picture. P_1 is the location of the nozzle exit and P_2 the position of the cylindrical body. For $\phi=3$, the compression region of the black area and the expansion region

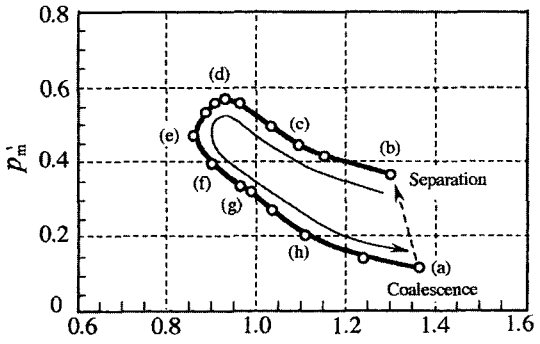

(a) p_m' vs x_m/D_e

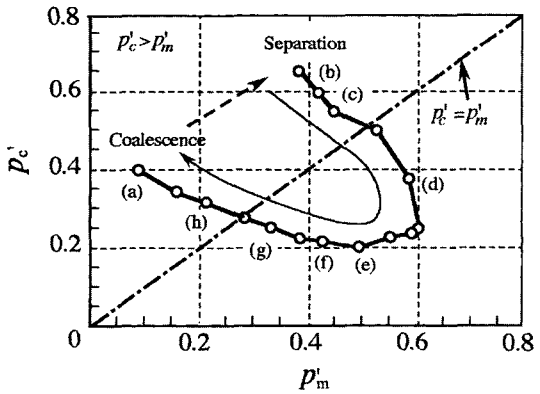

(b) p_m' vs p_c'

Fig. 9 Relationship among p_m', x_m/D_e and p_c' ($x_c/D_e=2.0$ and $\phi=5.5$)

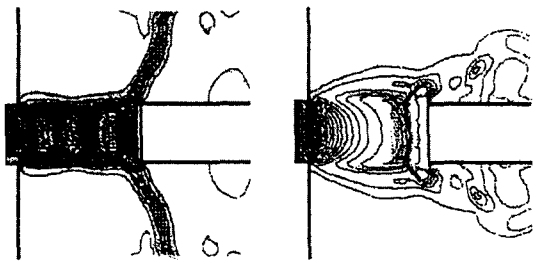

(a) $\phi=3.0$ (b) 9.0

Fig. 10 Computed density contours for $\phi=3.0$ and $9.0(x_c/D_e=2.0)$

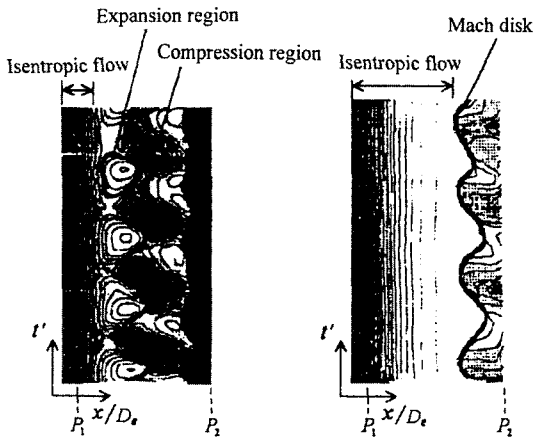

(a) $\phi=3.0$ (b) $\phi=9.0$

Fig. 11 Time variation of pressure distribution on the nozzle axis$(x_c/D_e=2.0)$

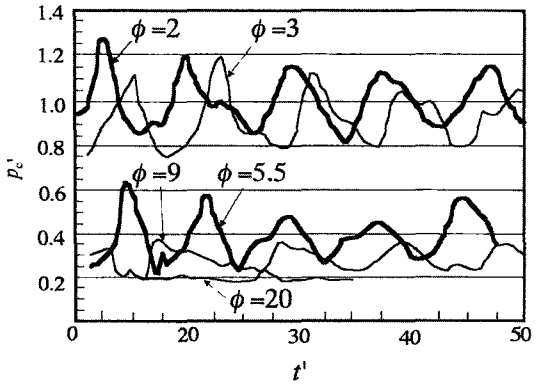

Fig. 12 Time variation of stagnation pressures p_c' $(x_c/D_e=2.0)$

of the light area are repeated regularly. The position of the compression region in front of the cylindrical body seems to slightly vary with time. For $\phi=9$, it is observed that the Mach disk oscillates regularly around a time-mean position and its amplitude is larger, compared with that of $\phi=3$. In this case, the plate shock wave does not occur.

Figure 12 shows the predicted time histories of the pressure p_c' at the stagnation point on the cylindrical body. For $\phi=3$, in which the cell-structures appear to be repeated, it seems that p_c' oscillates between 0.8 and 1.2, but for $\phi=5.5$, it varies between 0.2 and 0.64. It is known that the variation of p_c' decreases with an increase in ϕ, and at $\phi=20$, the variation of p_c' seems to nearly disappear, leading to no any appreciable self-induced oscillations.

5. Conclusions

The self-induced oscillations of the underexpanded sonic jet impinging on a cylindrical body were investigated by flow visualizations and computational analyses. The detailed characteristics of the Mach disk motions and the resulting pressure variations along the nozzle axis were elucidated. The major conclusions obtained are summarized as follows:

(1) Depending on the pressure ratios, the self-induced oscillation occurs when the cylindrical body x_c locates between $2D_e$ and $3.5D_e$. At $x_c=2D_e$, the pressure ratio for the self-induced oscillations is in the range of $5\leq\phi\leq9$ and at $x_c=3D_e$ it is $9\leq\phi\leq13$. The pressure ratio in which the self-induced oscillations occur increases with x_c/D_e.

(2) The position x_m/x_c of the Mach disk increases with the pressure ratio ϕ and it decreases as the position x_c/D_e of the cylindrical body increases. The present computations predict these experimental results with fairly good accuracy.

(3) The formation of the plate shock wave in front of a cylindrical body is due to coalescence of the Mach disk with the compression region downstream of the Mach disk. The pressure p_c' at the stagnation point of the cylindrical body and its variation range decrease with an increase in ϕ. For $\phi=20$, there are no any appreciable self-induced oscillations.

(4) The pressure p_c' at the stagnation point of the cylindrical body and the diameter of the Mach disk strongly depend on the position of the Mach disk and on its movement path as well.

(5) The self-induced oscillations of the under-expanded sonic jet impinging upon a cylindrical body are generated by unbalance of the pressure in the flow.

Acknowledgment

This work was supported by the Brain Korea 21 project in 2001.

References

Addy, A. L., 1981, "Effects of Axisymmetric Sonic Nozzle Geometry on Mach Disk Characteristics," *AIAA Journal*, Vol. 19, No. 1, pp. 121~122.

Gummer, J. H. and Hunt, B. L., 1974, "The Impingement of Non-Uniform, Axisymmetric, Supersonic Jets on a Perpendicular Flat Plate," *Israel J. Tech.*, Vol. 12, pp. 221~235.

Iwamoto, J., 1990, "Impingement of Under-Expanded Jets on a Flat Plate," *ASME J. Fluids Eng.*, Vol. 112, pp. 179~184.

Jennions, I. K. and Hunt, B. L., 1980, "The

Axisymmetric Impingement of Supersonic Air Jets on Cones," *Aeronautical Quarterly*, Feb., pp. 26~39.

Jungowski, W. M., 1978, "Some Self-Induced Supersonic Flow Oscillations," *Progress in Aerospace Sciences*, Vol. 18, pp. 151~175.

Kim, H. D. and Matsuo, K., 1992, "Measurement of Oscillating Shock Wave in Supersonic Nozzle," *Proceedings of 6th International Symposium on Flow Visualization*, pp. 612~616.

Kim, H. D., Kashiumra, H. and Setoguchi, T., 2001a, "Suppression of the Self-Induced Oscillations of the Underexpanded Jets Impinging upon an Object," 8th *International Symp. on Sound and Vibration*, June, 2001, Hongkong.

Kim, H. D., Lee, K. H. and Setoguchi, T., 2001b, "Study of the Supersonic Dual Coaxal Jets," *40th AIAA Aerospace Sciences Meeting*, Reno, Nevada, Jan 2002 (submitted).

Lamont, P. J. and Hunt, B. L., 1980, "The Impingement of Underexpanded, Axisymmetric Jet on Perpendicular and Inclined Flat Plates," *J. Fluid Mech.*, Vol. 100, Part 3, pp. 471~511.

Nishida, M. and Matsumura, Y., 1994, "Numerical Simulation of a Supersonic Free Jet Impingement on a Flat Plate," *Computational Fluid Dynamics*, Vol. 3, pp. 175~186.

Powell, A., 1988, "The Sound-Producing Oscillation of Round Underexpanded Jets Impinging on Normal Plates," *J. Acoust. Soc. America*, Vol. 83, No. 2, pp. 515~533.

Sod, G. A., 1977, "A Numerical Study of a Converging Cylindrical Shock," *J. Fluid Mech.*, Vol. 83, Part 4, pp. 785~794.

Yee, H. C., 1987, "Upwind and Symmetric Shock-Capturing Schemes," *NASA TM* 89464, pp. 1~127.